Sixteen International Water Technology Conference, IWTC16 2012, Istanbul, Turkey

A hybrid solar desalination system of air humidification dehumidification and water flashing evaporation Part I. A numerical investigation

A. E. Kabeel

Professor
Mechanical Power Engineering Department
Faculty of Engineering
Tanta University
Tanta, Egypt

E-mail: kabeel6@hotmail.com

Emad M. S. El-Said

M.Sc. Engineer
Mechanical Power Engineering Department
Faculty of Engineering
Tanta University
Tanta, Egypt

E-mail: emad_mech@hotmail.com

Abstract

This paper presents a hybrid solar desalination system consisting of a humidification dehumidification unit and single stage flashing evaporation unit. The hybrid solar desalination system was studied numerically. The heat and mass transfer and flow field is modeled theoretically in two-dimensional using finite difference scheme. For different operating and weather conditions the fresh water productivity and salinity are computed. The model is developed to investigate the steady-state behavior of each component of the system. The results show that, the studied hybrid desalination system give a significant operational compatibility between the air humidification dehumidification method and flash evaporation desalination.

Keywords: Humidification/Dehumidification; Flashing desalination; Hybrid.

1. Introduction

Egypt and the surrounding MEDA and other regional countries have exceeded the so called water poverty level. The situation is not better in the other nearby courtiers in MENA and EU. The standard high capacity desalination methods such as multi-stage flash evaporation and multi-effect evaporation, vapor compression and reverse osmosis are reliable in the range of some 100-500,000 m^3/d fresh water productions. However, the wide-scale implementation of these technologies faces numerous technological, economic and policy barriers and they are not used in decentralized regions with a poor infrastructure due to their permanent need of qualified maintenance and electricity supply. Desalination units of solar energy driven are a promising technique for the production of fresh water in remote and sunny regions. The desalination process of "humidification-dehumidification" (HDH) becomes a feasible solution to future freshwater shortages operates at near-ambient pressure and low temperature and can be driven by solar energy as well as a variety of low-grade (low-temperature) thermal-energy sources including low-pressure condensing steam from steam power plants, waste heat from combustion

engines. Shaobo Hou et al. [2008] studied the hybrid solar desalination process of the multi effect humidification–dehumidification and the basin type unit. The gain output ratio of this system was raised by 2–3 at least through reusing the rejected water. Garg et al. [2002] presented an experimental design and computer simulation of multi effect humidification–dehumidification solar desalination and the developed model which is useful in the estimation of the distillation plant output and optimized various components of the system like, solar water heater, humidification chamber, and condensation chamber. G. Prakash Narayan et al. [2010] analyze the thermodynamic performance of various humidification and dehumidification cycles by way of a theoretical cycle analysis. Propose novel high-performance variations on those cycles. These high performance cycles include multi-extraction, multi-pressure and thermal vapor compression cycles. The Gained Output Ratio (GOR) of the systems based on these novel cycles excess of 7 and will outperform existing humidification and dehumidification systems.

Thermodynamically, flash evaporation occurs when a saturated liquid undergoes a sudden reduction in the surrounding pressure so that a part of the liquid immediately turns to vapor to regain equilibrium; under adiabatic conditions, the generated vapor receives its latent heat of vaporization at the expenses of the surrounding liquid and both the vapor and the residual liquid are cooled to the saturation temperature at the reduced pressure. A.S. Nafey et al. [2007] investigate theoretically and experimentally a small unit for water desalination by solar energy and a flash evaporation process at different real environmental conditions. The system consists of a solar water heater (flat plate solar collector) working as a brine heater and a vertical flash unit that is attached with a condenser/preheater unit. The mathematical model is developed to calculate the productivity of the system under different operating conditions. Comparison between the theoretical and experimental results is performed. The average accumulative productivity of the system ranged between 1.04 to 1.45 kg/day/m^2. The average summer productivity ranged between 5.44 to 7 kg/day/m^2 and 4.2 to 5 kg/day/m^2. Hasan Baig et al. [2010] investigate the effect of various operating conditions on the performance ratio, brine temperature and salinity as it leaves the last flash stage are d in a once-through the multi-stage flash (MSF) distillation system. Use reliable correlations for calculating brine properties that vary with both temperature and salinity. Compared the numerical results obtained with the published data on similar plants. A sensitivity analysis to identify the key parameters that significantly influence the desalination plant performance is carried out in an attempt to contribute a better understanding on modeling and optimum operation of MSF desalination processes. Both analytical solutions and experimental/field analysis are required to identify the most influential parameters that affect the performance and set proper plans for performance optimization. The accurate estimate of the variables related to the brine heater, selecting proper number of stages and the stage-to-stage temperature drop are of crucial importance. The thermal properties dependent on the operating conditions may affect the accuracy of numerical results. The salinity of the

feed seawater has a significant effect on the plant characteristics. Y. Junjie et al. [2010] study experimentally the heat and mass transfer properties of static/circulatory flash evaporation, i.e., nonequilibrium fraction (NEF), evaporated mass and heat transfer coefficient. The heat transfer coefficient was redefined as average heat flux released from unit volume of water film under unit superheat. Results suggested that this coefficient was a time-depended function and a peak value existed in its evolution versus time. Mohammad Abutayeh and D. Yogi Goswami [2009] Simulate theoretical and experimentally a passive vacuum flash desalination system. The system consists of a saline water tank, a concentrated brine tank, and a fresh water tank placed on ground level plus an evaporator and a condenser located several meters above the ground. The evaporator condenser assembly, or flash chamber, is initially filled with saline water that later drops by gravity, creating a vacuum above the water surface in the unit without a vacuum pump. The vacuum is maintained by the internal hydrostatic pressure balanced by the atmospheric pressure. The ground tanks are open to the atmosphere, while the flash chamber is insulated and sealed to retain both heat and vacuum. The simulation results show that running the system at higher flash temperatures with a fixed flash chamber size will result in faster vacuum erosion leading to less overall evaporation.

2. System process model

The system consists of two parts. One is a solar HDH unit, and another is a single-stage flashing evaporation (SSF) unit. A sketch of a hybrid solar desalination process of the humidification dehumidification and the single stage flashing evaporation unit is shown in Fig.1. The solar HDH unit consists of humidifier, condenser (dehumidifier), and heating sources (water heater nano-fluid solar collector and air heater solar collector). The unit is operated in a forced draft mode by using an air blower and with a closed loop for air circulation. A packing is used in the humidifiers for efficient humidification of the air. The feed water at (10) is sprayed over the packing in the humidifier. The air at (17) is heated in air flat plate solar collector and out at (11). The air at (11) is humidified in the humidifier and out at (12). The brine at (13) is pumped to mixing tank. The saline water at (14) is fed to the dehumidifier to condense the water vapor from the air at (12). The air at (16) is which got at the bottom of the condenser return to the solar air heater to reheat and complete the closed air cycle. The fresh desalinated water at (16) is collected from the bottom of the condenser.

The solar SSF unit consists of flashing chamber and condenser. The warm saline water flowed from mixing tank at (18) is reheated in heat exchanger by the heat from nano-fluid flat plate solar collector and desalinated in a single-stage flashing distill unit to distill water further. The water at (3) is pumped to flashing chamber to evaporate by flashing. The extracted water vapor on flashing chamber is flowed to the condenser. The saline water at (6) is fed to the flashing unit condenser to condense the water vapor and out at (7). The desalinated water at (8) is collected from the bottom of the condenser tray, while is rejected from the bottom of the condenser tray. The flashing evaporation depends

on the pressure reduction. So, the inside the condenser and flashing chamber is vacuumed by using vacuum pump at (9).

Then, the saline water out from two condensers (C1) and (C2) at (7) and (15) respectively, is mixed with rejected brine water from humidifier and flashing chamber at (13) and (4) respectively, in mixing tank as will as is further preheated the feed water to (18) and (10). Increasing the temperature of water in the conventional HDH process increases the solubility of the different salts as indicated by Dean [2001], which causes some difficulties in desalination operation. In the present system heating inlet air instead of seawater reduces this phenomenon.

3. System Mathematical modeling

The mathematical model in the steady state regime allows determining the coupling equations between the water temperature, the humid air temperature and water content inside each component. The water salinity will be considered. The energy balance equation can be written for the entire system in the following manner, by taking input energy terms equal to output energy terms:

3.1 Humidifier modeling

The humidifier may be modeled as shown in Fig. 2. Air flow rates enter the bottom of the humidifier at a temperature $T_{a,in,ev}$ and humidity $\omega_{a,in,ev}$. The mass flow rate of air is $\dot{m}_{a,ev}$. The air flow rates exit at the top of the humidifier at a temperature $T_{a,o,ev}$ and a humidity $\omega_{a,o,ev}$. Salt water is pulverized at the top of the humidifier with a temperature $T_{w,o,ev}$ and no evaporated water is in the bottom of the humidifier with a temperature $T_{w,o,ev}$. The mass flow rate of water is $\dot{m}_{w,o,ev}$.

The formulation of the mathematical model is obtained by applying the thermal and mass transfers on an element of volume of height *dy* as presented in Fig. 2. For the humidifier packing bed cross-sectional area $A_{cs,ev}$ and $H_{p,ev}$ height, the steady mass flow rate of dry air per unit cross-sectional area is

$$M_{a,ev} = \frac{\dot{m}_{a,ev}}{A_{cs,ev}} \quad \text{……...…….……} \quad (1)$$

And the corresponding mass flux of water flowing parallel with the air is

$$M_{w,ev} = \frac{\dot{m}_{w,ev}}{A_{cs,ev}} \quad \text{……...…….…….....…..…} \quad (2)$$

If $a_{H,,ev}$ and $a_{M,ev}$ are the area of heat transfer and mass transfer surface per unit of packing volume, respectively, the total surface areas for heat and mass transfer are:

$$A_{H,ev} = H_{P,ev} a_{H,ev} A_{cs,ev} \quad \text{and} \quad A_{M,ev} = H_{P,ev} a_{M,ev} A_{cs,ev} \quad \text{……...……..} \quad (3)$$

The basic equations for the process occurring in the differential length *dy* can be written as following.

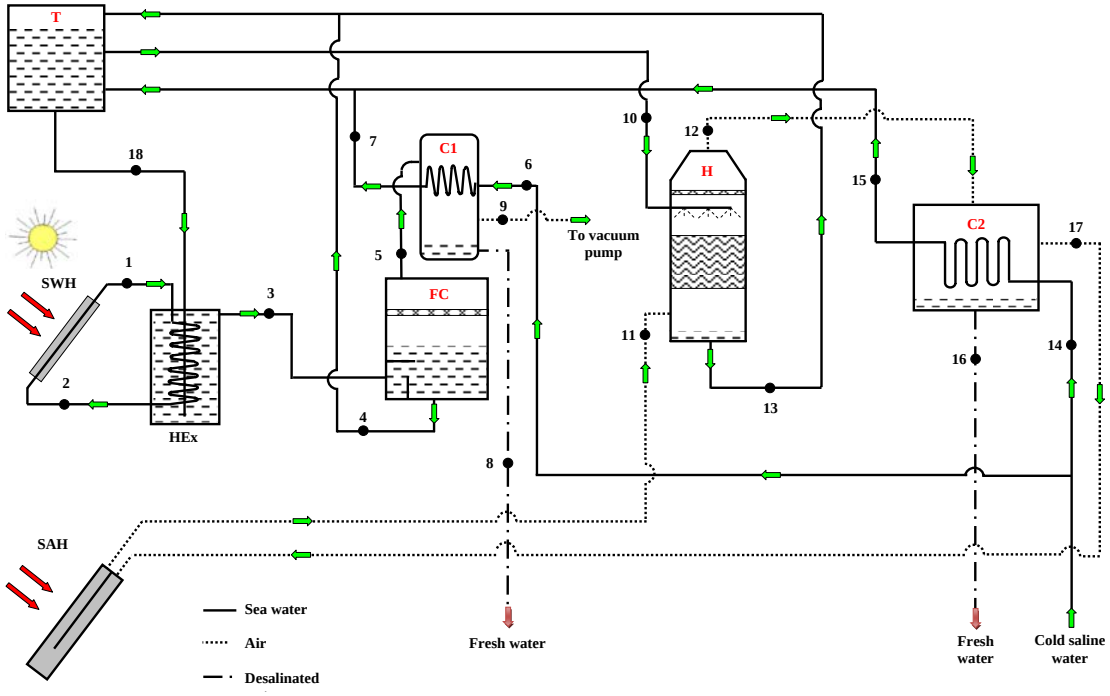

1.	T:	Mixing tank	5.	C1:	Flashing unit condenser
2.	SWH:	Solar water heater	6.	FC:	Flashing chamber
3.	Hex:	Heat exchanger	7.	H:	Humidifier
4.	SAH:	Solar air heater	8.	C2:	Dehumidifier

Fig. 1. Schematic diagram of (HDH/SSF) system.

Mass balance for humid air:

The mass balance equation of the amount of evaporated water into air yields:

$$dM_{w,ev} = M_{a,ev} d\omega_{a,ev} \quad \text{..... (4)}$$

The mass of air changes due to the amount of vapor that gets suspended in it as it flows inside the humidifier. Since the rate of dry air is constant, the evaporation rate in the element is expressed as:

$$M_{a,ev} d\omega_{a,ev} = k_{L,ev}\, \rho_{a,ev}\, a_{H,ev} \left(\omega_{i,ev} - \omega_{a,ev}\right) dy \quad \text{..... (5)}$$

Rearranging Equation (5):

$$\frac{d\omega_{a,ev}}{dy} = \frac{k_{L,ev}\, \rho_{a,ev}\, a_{H,ev} \left(\omega_{i,ev} - \omega_{a,ev}\right)}{M_{a,ev}} \quad \text{..... (6)}$$

Heat transfer to air

A closer look at Fig.3 shows that heat is being transferred from the air stream to the surface of the liquid film on the packing. At the same time water vapor evaporates from

the interface and is diffused into the air stream. Further it is assumed that all resistant for heat transfer lies on the gas side. That means big value for heat transfer coefficient on the water side and small value on gas side.

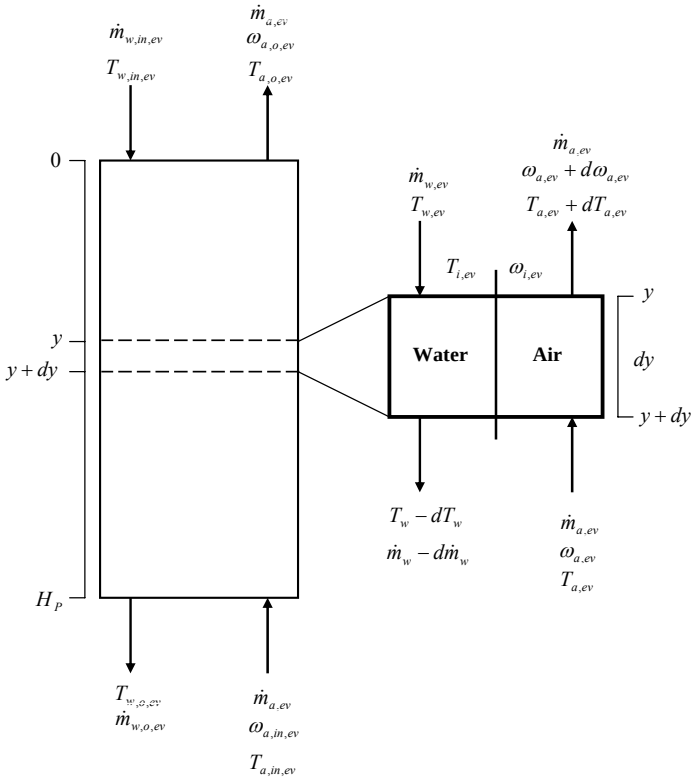

Fig.2. An element of the humidifier packing.

The sensible heat transfer between liquid and gas within the element *dy*, illustrated in Fig.2 is given by:

$$\frac{dT_{a,ev}}{dy} = \frac{h_{a,ev} a_{H,ev} \left(T_{i,ev} - T_{a,ev}\right)}{M_{a,ev} C_{P,ha,ev}} \quad \text{..... (7)}$$

Where:

$$C_{p,ha,ev} = C_{p,a,ev} + \omega_{a,ev} C_{p,v,ev} \quad \text{..... (8)}$$

Energy balance for water:

Equating the energy at water side leads to:

$$M_{w,ev} C_{p,w,ev} \frac{dT_{w,ev}}{dy} = h_{w,ev} a_{M,ev} \left(T_w - T_i\right) \quad \text{..... (9)}$$

i.e.

$$\frac{dT_{w,ev}}{dy} = \frac{h_{w,ev} a_{M,ev} \left(T_w - T_i\right)}{M_{w,ev} C_{p,w,ev}} \quad \text{..... (10)}$$

Energy balance for humid air:

The air exchanges heat by convection with water in addition to the heat from the vapor. This heat results in changing the enthalpy of the air stream. The air stream is composed of dry air accompanied by water vapor. The direction of air flow is opposite to the direction of water flow. Since, the total amount of thermal energy gained is the sum of the thermal energy for the phase change, Q_{evap} (evaporation) and the thermal energy for the temperature change, Q_{w-a}.

$$\frac{d}{dy}\left(M_{ha,ev} i_{ha,ev}\right) = Q_{w-a} + Q_{evap} \quad \text{..... (11)}$$

So, the humid air energy balance can be wrote in terms of the heat and mass transfer coefficients, h_a and k_a, respectively, as

$$\frac{d}{dy}\left(M_{ha,ev} i_{ha,ev}\right) = h_{a,ev} a_{H,ev}\left(T_{i,ev} - T_{a,ev}\right) + k_{L,ev}\, \rho_{a,ev} a_{H,ev} \lambda_{fg,ev}\left(\omega_{i,ev} - \omega_{a,ev}\right) \quad \text{..... (12)}$$

Enthalpy of the humid air is:

$$M_{ha,ev} i_{ha,ev} = M_{a,ev} i_{a,ev} + M_{v,ev} i_{v,ev} \quad \text{..... (13)}$$

We note also that enthalpies for the water vapor and air are:

$$i_{v,ev} = C_{p,v,ev} T_{a,ev} + \lambda_{fg,ev} \quad \text{..... (14)}$$

$$i_a = C_{p,a} T_{a,ev} \quad \text{..... (15)}$$

Division by $M_{a,ev}$ on both sides of Eq. (13) will result in:

$$\frac{M_{ha,ev} i_{ha,ev}}{M_{a,ev}} = i_{a,ev} + \omega_{a,ev} i_{v,ev} \quad \text{..... (16)}$$

Where

$$\omega_{a,ev} = \frac{M_{v,ev}}{M_{a,ev}} \quad \text{..... (17)}$$

Eqs. (14), (15), (16) and (12) combined give:

$$\frac{M_{ha,ev} i_{ha,ev}}{M_{a,ev}} = C_{p,a,ev} T_{a,ev} + \omega_{a,ev} C_{p,v,ev} T_{a,ev} + \lambda_{fg,ev} \omega_{a,ev} \quad \text{..... (18)}$$

And substituting from Eq. (8) into Eq. (18) gives:

$$\frac{M_{ha,ev} i_{ha,ev}}{M_{a,ev}} = C_{p,ha,ev} T_{a,ev} + \lambda_{fg,ev} \omega_{a,ev} \quad \text{..... (19)}$$

And introducing Eq. (18) into Eq. (11) gives:

$$\frac{d}{dy}\left(M_{ha,ev} i_{ha,ev}\right) = M_{a,ev} C_{p,ha,ev} dT_{a,ev} + M_{a,ev} \lambda_{fg,,ev} d\omega_{a,ev} \quad \text{..... (20)}$$

Combining Eq. (19) and Eq. (12) gives:

$$M_{a,ev}\left(C_{p,ha,ev}\ dT_{a,ev}+\lambda_{fg,ev}d\omega_{a,ev}\right)=\begin{bmatrix}h_{a,ev}a_{H,ev}\left(T_{i,ev}-T_{a,ev}\right)+\\ k_{L,ev}\,\rho_{a,ev}\,a_{M,ev}\lambda_{fg,ev}\left(\omega_{i,ev}-\omega_{a,ev}\right)\end{bmatrix}dy \quad \text{..... (21)}$$

Differentiating the left hand side of Eq. (21) by *dy* leads to:

$$M_{a,ev}C_{p,ha,ev}\frac{dT_{a,ev}}{dy}+M_{a,ev}\lambda_{fg,ev}\frac{d\omega_{a,ev}}{dy}=h_{a,ev}a_{H,ev}\left(T_{i,ev}-T_{a,ev}\right)+ k_{L,ev}\,\rho_{a,ev}\,a_{M,ev}\lambda_{fg,ev}\left(\omega_{i,ev}-\omega_{a,ev}\right) \quad \text{..... (22)}$$

Mass balance for water:

$$\frac{dM_{w,ev}}{dy}=k_{L,ev}\,\rho_{w,ev}a_{M,ev}\left(\omega_{i,ev}-\omega_{a,ev}\right) \quad \text{..... (23)}$$

Salt mass balance for water:

The overall salt mass balance assumes that the distillate water is salt free. The balance equations are given by:

$$x_{w,in}\,\dot{m}_{w,in}=x_{w,o}\dot{m}_{w,o} \quad \text{..... (24)}$$

Mass Transfer Coefficients:

Since one-dimensional formulation is used, these equations require closure relationships. Specifically, the heat and mass transfer coefficients of the air and water sides are required. The transfer of a solute from water to air follows the two-film theory covering transfer from (1) bulk-water to water-film, (2) water-film to air-film, and (3) air-film to bulk-air. The rate at which a solute is transferred from water to air, for low solubility solutes, is represented by an overall mass transfer coefficient, k_L. For design purposes, k_L should be determined experimentally. However, for dilute solutions, k_L can be determined from the Sherwood and Holloway equation. The mass transfer coefficients associated with film flow in packed beds have been widely investigated. The most widely used and perhaps most reliable correlation is that proposed by Onda et al. [1968]. Onda's correlation is used to calculate the mass transfer coefficients in the humidifier, $k_{a,ev}$ and $k_{w,ev}$. However, it was found at Onda's correlation under-predicted the wetted specific area of the packing material. See Appendix for details.

3.2. Dehumidifier modeling

Coil tube falling film condenser with a configuration of in-line tube used as a dehumidifier, as shown in Fig.3, two fluids flow inside the dehumidifier. The air and the feed water are not in direct contact. The cooling water carries the heat from the humid air. The balances are done on an element of volume of the tower of height *dy*, Fig.7 shows the flow direction for the two streams inside the element. A steady-state mathematical formulation has been assumed and developed with thermal and mass balance in a similar manner to those for the humidifier. This formulation gives the coupling equations between the temperature of the cooling water of the dehumidifier and the humid air

temperature and water content. The humid air enters the dehumidifier by the top at temperature $T_{a,i,co}$, humidity ratio $\omega_{a,i,co}$ and mass flow rate $\dot{m}_{a,i,co}$. The cooling water is introduced at temperature $T_{w,i,co}$ and a mass flow rate $\dot{m}_{w,i,co}$ (Fig.4). In the dehumidifier the humid air moves down through the space between the tubes. On contact with the cold tube walls, there is film condensation coupled with latent heat restitution to the salt water circulating inside the tubes. The presence of a film creates a barrier between the vapor and the cooled surface and thus retards the condensation process. The humid air and liquid film flows are assumed to be approximately equal over the various channels of the heat exchanger. Because of the geometry of the condenser, the transfer between the fluids is a three-dimensional process. In fact, all the parameters characterizing heat and mass transfer vary from one tube to the other. To simplify the modeling, we consider the mean values of the temperature and water vapor mixed fraction in each tube. The modeling problem becomes one-dimensional. The regime considered in this investigation is permanent. For a typical element *dy*, the humid air and the condensed liquid film flow between the tubes and the cooled water flows inside the tubes in Y direction.

The positive direction is chosen downwards, thus the falling film has a positive velocity. The coordinates are rendered dimensionless by means of the tube cell height H_{co}. A fraction of the heat flux supplied by the condensation is transferred to the cooling water inside the tubes by conduction through the liquid film and the tube walls.

Energy balance for cooling water:

$$\frac{dT_{w,co}}{dy} = \frac{N_{coil,co}\pi d_{tube,in,co} U_{L,co}\left(T_{a,co} - T_{w,co}\right)}{\dot{m}_{w,co} C_{p,w,co}} \quad \text{..... (25)}$$

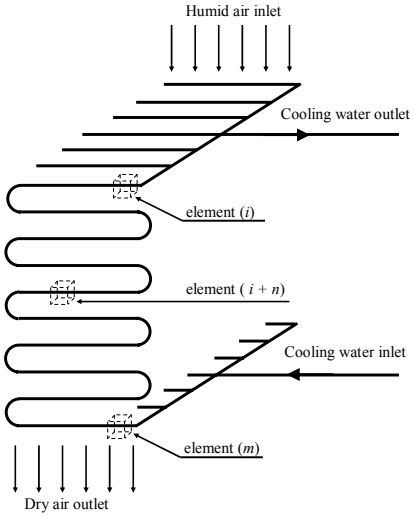

Fig.3 Dehumidifier schematic with flow streams.

The thermal resistances and overall heat transfer coefficient from the air to the cooling water inside the condenser is approximated by:

$$U_{L,co} = \frac{1}{\frac{1}{h_{a,co}} + \frac{1}{h_{cf,co}} + \frac{1}{h_{cw,iw,co}} + \frac{\delta_{tube,co}}{K_{tube,co}}} \quad \text{……...……...……} \quad (26)$$

Mass balance for humid air:

$$\frac{d\omega_{a,co}}{dy} = N_{coil,co}\pi d_{tube,o,co}\left[\frac{k_{co}\left(\omega_{a,co} - \omega_{i,co}\right)}{\dot{m}_{a,co}}\right] \quad \text{…….…...……..……...…} \quad (27)$$

Energy balance for humid air:

The rate of heat transfer from the vapor to the tube through the water film is simply equal to the heat in the amount λ_{fg} is released during condensation as the water vapor is condensed, the amount of heat for cooling of the liquid below the saturation temperature (subcooling) and heat for vapor cooling of vapor that enters the condenser as superheated vapor. The energy balance yields:

$$C_{p,ha,co}\frac{dT_{a,co}}{dy} + \lambda_{fg,co}\frac{d\omega_{a,co}}{dy} = \frac{N_{coil,co}\pi d_{tube,o,co}}{\dot{m}_{a,co}}\begin{bmatrix} h_{a,co}\left(T_{a,co} - T_{i,co}\right) + \\ k_{co}\lambda_{fg,co}\left(\omega_{a,co} - \omega_{i,co}\right)\end{bmatrix} \quad \text{…….……} \quad (28)$$

Condensation productivity:

The condensation rate is determined using an algebraic equation that relates the variation of the water content along the height of the dehumidifier:

$$d\dot{m}_{dis} = \dot{m}_{a,co}\, d\omega_{a,co} \quad \text{……..……...…} \quad (29)$$

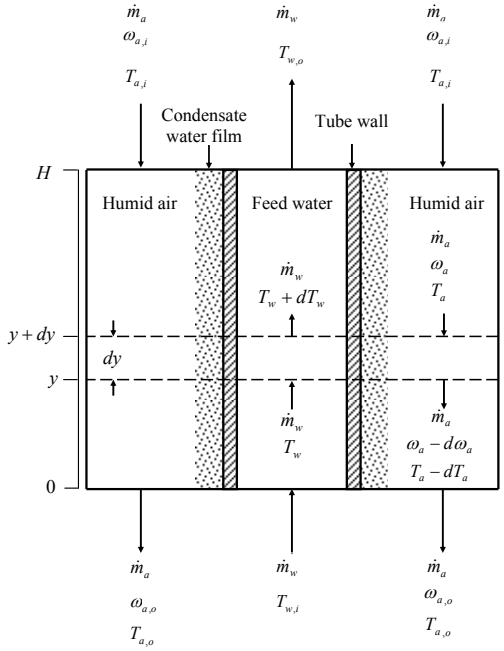

Fig.4 An element of the dehumidifier and temperature and humidity profile near tube at condensed film.

3.3. Flat plate solar water heater modeling

Flat plate solar collector is used to heat nano-fluid. Under steady-state conditions, the rate of useful heat delivered by a solar collector is equal to the rate of energy absorbed by the heat transfer fluid minus the direct or indirect heat losses from the surface to the surroundings.

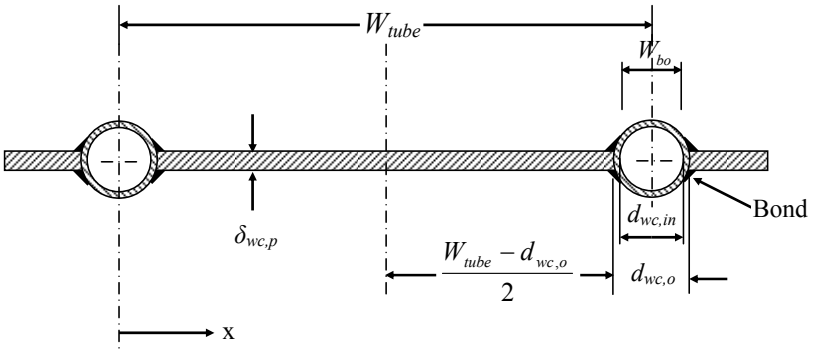

Fig.5. Sheet and tube dimensions of flat plat solar collector.

The energy conducted to the region of the tube per unit length in the flow for both sides is:

$$q'_p = \left(W_{tube} - d_{wc,o}\right)F\left[S - U_{L,wc}\left(T_{wc,p} - T_{am}\right)\right] \quad \text{(30)}$$

Where

$$F = \frac{\tanh\left[\Gamma\left(W_{tube} - d_{wc,o}\right)/2\right]}{\Gamma\left(W_{tube} - d_{wc,o}\right)/2} \quad \text{(31)}$$

The useful gain of the collector also includes the energy collected above the tube region. This is given by

$$q'_{tube} = d_{wc,o}\left[S - U_{L,wc}\left(T_{wc,p} - T_{am}\right)\right] \quad \text{(32)}$$

Accordingly, the useful energy gain per unit length in the direction of the fluid flow is

$$q'_u = q'_p + q'_{tube} = \left[\left(W_{tube} - d_{wc,o}\right)F + d_{wc,o}\right]\left[S - U_{L,wc}\left(T_{wc,p} - T_{am}\right)\right] \quad \text{(33)}$$

This energy ultimately must be transferred to the fluid, which can be expressed in terms of two resistances as

$$q'_u = \frac{T_{wc,p} - T_{nf,wc}}{\frac{1}{h_{nf,wc,in}\,\pi\, d_{wc,in}} + \frac{1}{C_{bo}}} \quad \text{(34)}$$

In Eq. (33), C_{bo} is the bond conductance, which can be estimated from knowledge of the bond thermal conductivity, (K_{bo}), the average bond thickness, (δ_{bo}), and the bond width, (W_{bo}). The bond conductance on a per unit length basis is given by

$$C_{bo} = \frac{K_{bo} W_{bo}}{\delta_{bo}} \quad \text{..... (35)}$$

To obtain an expression for the useful gain in terms of known dimension, physical parameters, and fluid temperature, ($T_{nf,wc}$) must eliminate. So, Solving Eq. (33) for, ($T_{wc,p}$), substituting it into Eq. (32), and solving the resultant equation for the useful gain, we get

$$q'_u = W_{tube} F' \left[S - U_{L,wc} \left(T_{nf,wc} - T_{am} \right) \right] \quad \text{..... (36)}$$

Where

$$F' = \frac{\dfrac{1}{U_{L,wc}}}{W_{tube} \left\{ \dfrac{1}{U_{L,wc} \left[d_{wc,o} + F \left(W_{tube} - d_{wc,o} \right) \right]} + \dfrac{1}{C_{bo}} + \dfrac{1}{h_{nf,wc,in} \pi d_{wc,in}} \right\}} \quad \text{..... (37)}$$

Consider an infinitesimal length (*dy*) of the tube. The useful energy delivered to the fluid is $q'_u dy$. Under steady-state conditions, an energy balance for n tubes gives:

$$q'_u \, dy + \frac{\dot{m}_{nf,wc}}{N_{wc,tube}} C_{p,nf} T_{nf,wc} - \frac{\dot{m}_{nf}}{N_{wc,tube}} C_{p,nf} \left(T_{nf,wc} + \frac{dT_{nf,wc}}{dy} dy \right) = 0 \quad \text{..... (38)}$$

Dividing through by (*dy*), finding the limit as (*dy*) approaches 0, and substituting Eq. (36) results in the following differential equation:

$$\dot{m}_{nf,wc} C_{p,nf} \frac{dT_{nf,wc}}{dy} - N_{wc,tube} W_{tube} F' \left[S - U_{L,wc} \left(T_{nf,wc} - T_{am} \right) \right] = 0 \quad \text{..... (39)}$$

Assuming variables F' , $U_{L,wc}$, and $C_{p,nf}$ to be constants and performing the integration gives:

$$\ln \left(\frac{T_{nf,wc,o} - T_{am} - \left(S / U_{L,wc} \right)}{T_{nf,wc,in} - T_{am} - \left(S / U_{L,wc} \right)} \right) = - \frac{N_{wc,tube} W_{wc} L_{coil,wc} F' U_{L,wc}}{\dot{m}_{nf,wc} C_{p,nf}} \quad \text{..... (40)}$$

Where

$$A_{eff} = N_{wc,tube} W_{tube} L_{tube,wc}$$

Substituting by (A_{wc}) in Eq. (40), the following equation is obtained

$$\frac{T_{nf,wc,o} - T_{am} - \left(S / U_{L,wc} \right)}{T_{nf,wc,in} - T_{am} - \left(S / U_{L,wc} \right)} = \exp \left(- \frac{A_{eff} F' U_{L,wc}}{\dot{m}_{nf,wc} C_{p,nf}} \right) \quad \text{..... (41)}$$

Then

$$T_{nf,wc,o} = \left[T_{nf,wc,in} - T_{am} - \left(S / U_{L,wc} \right) \right] \left[\exp \left(- \frac{A_{eff} F' U_{L,wc}}{\dot{m}_{nf,wc} C_{p,nf}} \right) \right] + T_{am} + \left(S / U_{L,wc} \right) \quad \text{... (42)}$$

3.4 Solar air heater modeling

Flat plate solar collector is used to heat air with design of double pass double duct and double glass cover as shown in Fig.6. The steady-state energy balance on the cover, the plate and the fluid in the upper and lower ducts gives the following equations:

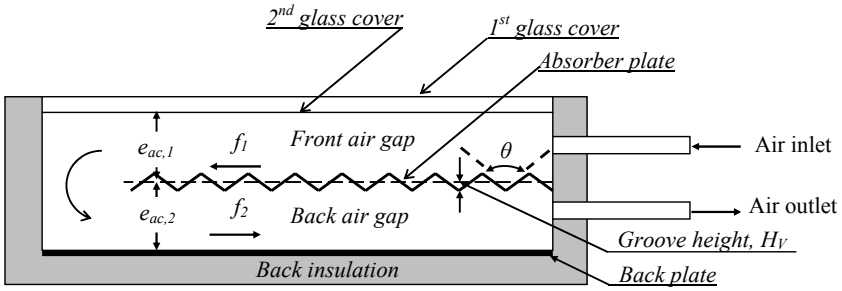

Fig.6 The structure of the air heater.

The top layer of glass cover:

$$U_t\left(T_{g1}-T_{am}\right)=h_{r,g2-g1}\left(T_{g2}-T_{g1}\right) \quad \text{(43)}$$

The Lower layer of glass cover:

$$h_{c,f1-g2}\left(T_{f1}-T_{g2}\right)+h_{r,p-g2}\left(T_p-T_{g2}\right)=h_{r,g2-g1}\left(T_{g2}-T_{g1}\right) \quad \text{(44)}$$

The heat absorbing plate:

$$S=h_{c,p-f1}\left(T_p-T_{f1}\right)+h_{c,p-f2}\left(T_p-T_{f2}\right)+h_{r,p-g2}\left(T_p-T_{g2}\right)+h_{r,p-b}\left(T_p-T_b\right) \quad \text{(45)}$$

Insulation bottom board:

$$U_b\left(T_b-T_{am}\right)=h_{r,p-b}\left(T_p-T_b\right)+h_{c,f2-b}\left(T_{f2}-T_b\right) \quad \text{(46)}$$

The heat transfer capacity between heat-absorbing plate and the air of the top channel (q_{u1}):

$$q_{u1}=h_{c,p-f1}\left(T_p-T_{f1}\right)+h_{c,f1-g2}\left(T_{g2}-T_{f1}\right) \quad \text{(47)}$$

The heat transfer capacity between heat-absorbing plate and the air of the lower channel (q_{u2}):

$$q_{u2}=h_{c,p-f2}\left(T_p-T_{f2}\right)+h_{c,f2-b}\left(T_b-T_{f2}\right) \quad \text{(48)}$$

Based on equation (47) and (49) (q_u) the heat transfer capacity between the air and heat absorbing plate can be calculated by the following formula (q_u):

$$q_u=h_{c,p-f1}\left(T_p-T_{f1}\right)+h_{c,f1-g2}\left(T_{g2}-T_{f1}\right)+h_{c,p-f2}\left(T_p-T_{f2}\right)+h_{c,f2-b}\left(T_b-T_{f2}\right) \quad \text{(49)}$$

And

$$q_u=\dot{m}_a c_{p,a}\left(T_{fo}-T_{fi}\right) \quad \text{(50)}$$

By combination Eq. (49) and Eq. (50) gives:

$$\dot{m}_a c_{p,a}\left(T_{fo}-T_{fi}\right)=h_{c,p-f1}\left(T_p-T_{f1}\right)+h_{c,f1-g2}\left(T_{g2}-T_{f1}\right)+h_{c,p-f2}\left(T_p-T_{f2}\right)+h_{c,f2-b}\left(T_b-T_{f2}\right) \quad \text{(51)}$$

To compute the air temperature of inlet and outlet of air heater, $T_{f,in}$ and $T_{f,out}$ .It is assumed that the average temperature of air in the collector is (T_f) and expressed as:

$$T_{f1} = T_{f2} = T_f = \frac{T_{f,in} + T_{f,o}}{2} \quad \text{..... (52)}$$

3.5. Single stage flashing unit modeling

The mathematical model for the single flash unit is simple and it includes total mass and salt mass balances, rate equations for the heat transfer units, as well as energy balances for the condenser.

Flashing pool model

Fig. 8 shows the schematic diagram of the flashing pool section, the mass and heat balances are given by:

Total mass and salt mass balances:

$$\dot{m}_{fw,fu} = \dot{m}_{b,fu} + \dot{m}_{dis,fu} \quad \text{..... (53)}$$

$$x_{fw,fu}\,\dot{m}_{fw,fu} = x_{b,fu}\dot{m}_{b,fu} \quad \text{..... (54)}$$

Eq. (54) assumes that the salt concentration, (x_{dw}), in the formed vapor is zero.

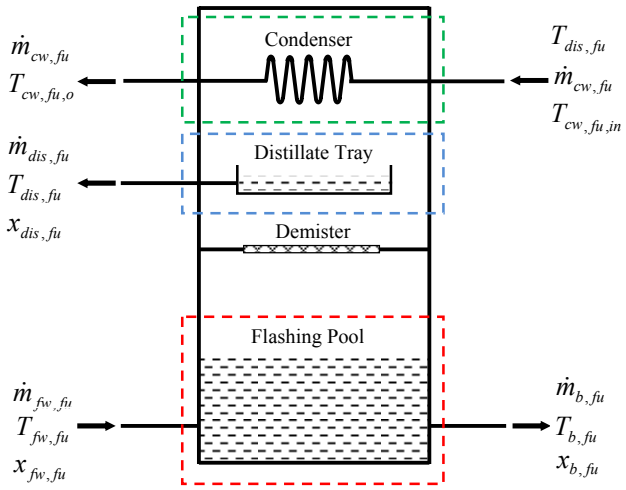

Fig. 7 Single stage flash desalination unit.

Energy balance:

As shown in Fig.8 the energy balance for the flashing brine is expressed as follows:

$$\dot{m}_{fw,fu}\, i_{fw,fu} = \dot{m}_{b,fu}\, i_{b,fu} + \dot{m}_{dis,fu}\, \lambda_{v,fu} \quad \text{..... (55)}$$

The brine is assumed to leave the flashing pool at saturation condition, and is calculated as a function of temperature and salinity of the exit brine conditions.

Condenser tube bundle model

Fig. 8 shows a schematic diagram of tube condenser bundle model section. The flashed

brine vapor and flashed distillate vapor flow over the tube bundle in order to condense, where the condensate flows back to the distillate tray. The effect of pressure loss over the tube bundle on the heat transfer coefficient was neglected in this model. However, the effect of the pressure loss across the tube bundle on the energy balance was considered in the form of temperature drop. The condensate was considered as a saturated liquid. The effect of condensate sub-cooling on the energy balance was evaluated as function of sub-cooling temperature.

Energy balances:

$$\dot{m}_{dis,fu}\,\lambda_{v,fu} = \dot{m}_{cw,fu}\left(i_{cw,o,fu} - i_{cw,in,fu}\right) + \dot{m}_{dis,fu}\,i_{dis,fu} \quad \text{(56)}$$

The heat transfer rate equation for the condenser is

$$\dot{m}_{cw,fu}\left(i_{cw,o,fu} - i_{cw,in,fu}\right) = \dot{m}_{cw,fu}\,C_{p,cw,fu}\left(T_{cw,o,fu} - T_{cw,in,fu}\right) = U_{co,fu}\,A_{co,fu}\,(LMTD)_{co,fu} \quad \text{(57)}$$

Where

$$(LMTD)_{co,fu} = \frac{\left(T_{cw,o,fu} - T_{cw,in,fu}\right)}{\ln\left[\dfrac{\left(T_{v,fu} - T_{cw,in,fu}\right)}{\left(T_{v,fu} - T_{cw,o,fu}\right)}\right]} \quad \text{(58)}$$

From Eq. (57) and after a few steps of simplification; the following equation is obtained:

$$(1-C)T_{cw,in,fu} + C\,T_{v,fu} = T_{cw,o,fu} \quad \text{(59)}$$

Where

$$C = 1 - e^{NTU} \quad \text{and} \quad NTU = -\frac{U_{co,fu}\,A_{co,fu}}{\dot{m}_{cw,fu}\,C_{p,cw,fu}}$$

For the equilibrium correlation; the relation between the outlet brine temperature (T_b) and the condensation temperature of the vapor, (T_v). is presented by following equation, El-Dessouky et al. [2002].

$$T_{v,fu} = T_{b,fu} - NEA - BPE \quad \text{(60)}$$

The non-equilibrium allowance (*NEA*) and Boiling Point Elevation (*BPE*) are calculated by the equations from appendix.

The overall heat transfer coefficient between the condensing vapor and the circulating cooling water, ($U_{L,co,fu}$):

$$U_{L,co,fu} = \frac{1}{\dfrac{1}{h_{cf,fu}} + \dfrac{1}{h_{cw,iw,fu}} + \dfrac{\delta_{tube,fu}}{K_{tube,fu}}} \quad \text{(61)}$$

4. Mathematical programming model

The main constraints of the mathematical programming model of the solar HDH/SSF system were presented in the previous section. Algebraic equations are used in to the model in original form. But for applying the differential equations, firstly they should be formed as algebraic equations using the forward finite difference method to obtain the

required values for air and water temperature, air humidity, flow rates of air and water. So, each of humidifier and dehumidifier is divided into j = 10 equal intervals or elements, the differential equations are expressed as a set of nonlinear algebraic equations. For the iteration procedure, the inlet water temperature of the solar water heater and the inlet air temperature of the solar air heater are guessed. The calculation procedure then marches along the solar water heater, solar air heater, humidifier, dehumidifier and flashing chamber. The outlet temperature of each unit is taken as the input for the next one. Finally, the outlet water and air temperatures are compared with the guessed inlet temperatures. The water and air physical properties are calculated as functions of temperature. The values of solar intensity is calculated numerically through the day and used as initial conditions for solution. A computer code in MATLAB® is prepared to solve the nonlinear set of equations of several variables using Gauss–Seidel iteration method. The programming takes into account that the air flow is in a counter direction of water flow. The temperature of air and water as well as the air humidity ratio is obtained at each segment in order to calculate the temperature distribution along the flow direction. Iterative procedure is followed for each segment and the solution is assumed to converge until the following inequality is valid:

$$\left|T^{e}-T^{g}\right| \le 0.01 \quad \text{.....} \quad (76)$$

The iteration is continued until the physical properties of water and air are obtained at each segment as a function of the mean temperature in any iteration.

6. Results and discussion

There are nine effects of system operation parameters (feed water salinity, feed water flow rate of SSF unit, feed water flow rate of HDH unit, cooling water flow rate of SSF unit, cooling water flow rate of HDH unit, air flow rate, cooling water temperature, wind speed and ambient temperature) has a direct impacts on system overall productivity. The numerical results that presented in this section are computed for 12 hours of operation time period start at 06:00 AM until 18:00 PM on August for Tanta city. For the above different conditions, the accumulative productivity of both methods (HDH and SSF) numerically at the mentioned times and date according to operation conditions shown in table (1). The solar radiation rate is computed also numerically according to location and weather conditions of Tanta city site.

Table (1): operation conditions

$\dot{m}_{fw,ev}$ =	3.5 kg/s.	$\dot{m}_{a}$ =	0.1 kg/s.	u_{wn} =	2.5 m/s.
$\dot{m}_{fw,fu}$ =	0.03 kg/s.	$T_{cw,in}$ =	25°C.	T_{am} =	25 °C.
$\dot{m}_{cw,co}$ =	0.055 kg/s.	$\dot{m}_{cw,fu}$ =	0.01 kg/s.	$x_{w,in}$ =	2100 ppm

6.1. Accumulative productivity and solar radiation with time

Fig. 8 shows the fresh water accumulative production with change of the solar intensity in the day time. From Fig. 8, it can be seen that the fresh water accumulative system production increase with the solar intensity strengthening and the freshwater production reduce with the solar intensity weakening. The maximal water production occurs from 12 p.m. to 13 p.m. and its value is 1086 mL.

6.2. Feed water salinity effect

Figure (14) shows that increasing of feed water salinity has a negative effect on system productivity in both hybrid methods of system desalination (HDH and SSF), which makes it decreasing. This effect may be explained by two impacts for HDH and SSF. For SSF the increasing of salt concentration increase the thermodynamic losses such as boiling point elevation and nonequilibrium allowance that decrease the rate of extracted vapor from saline water as well as product fresh water. For HDH, results show an increase of the water salinity upon a decrease in the evaporation rate because of the presence of salts in water reduces the vapor pressure at any given temperature. This reduces the driving force for evaporation and the accompanying latent heat.

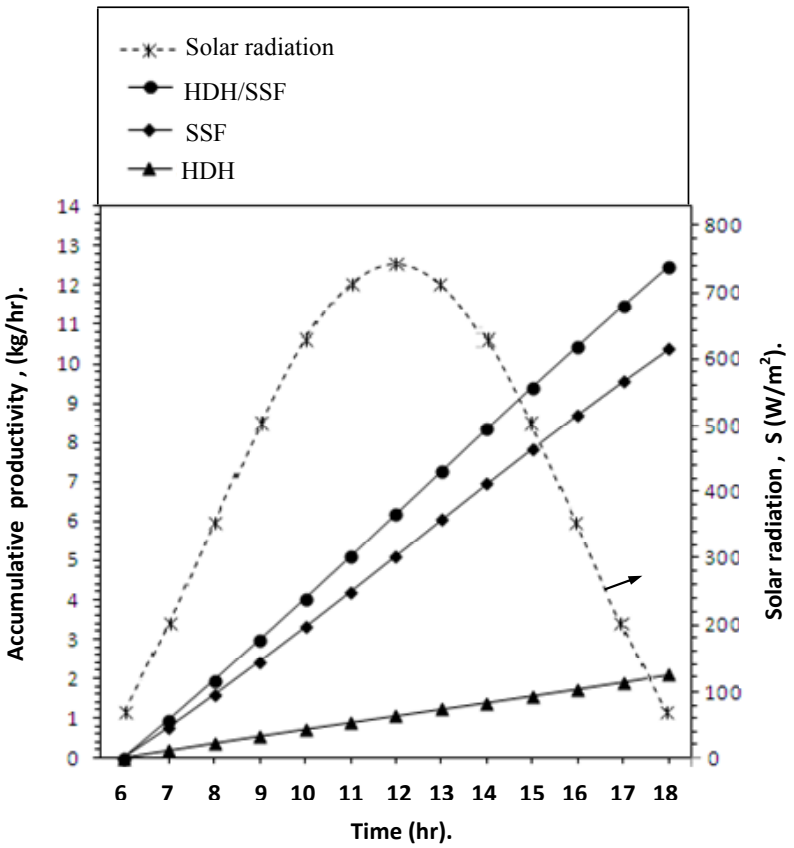

Fig. 8 Accumulative productivity and solar radiation during day hours.

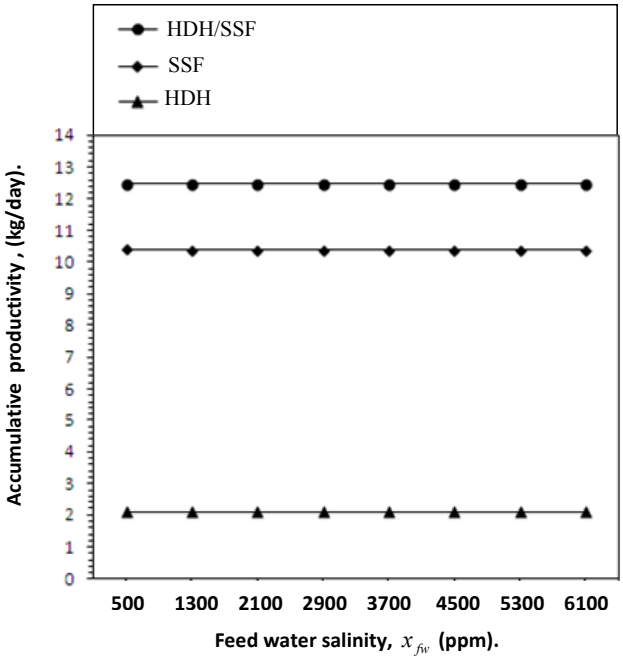

Fig. 9 Feed water salinity with accumulative productivity.

6.3. Feed water mass flow rate of SSF unit effect

The effect of the feed water mass flow rate of SSF unit on the hybrid system productivity is presented in Fig. 10. It shows that the productivity of the system decreases with increasing values of feed water mass flow rate of SSF unit. As shown in Fig. 10. the productivity of the HDH unit is not affected by change the value of feed water mass flow rate of SSF unit, which means that decreasing of hybrid system productivity is dependent only on the productivity of SSF unit. These may be explained as follows; by increasing the flow rate TBT of the SSF unit will decrease and then less the productivity of the unit.

6.4. Feed water mass flow rate of HDH unit effect

Fig. 11. present the effect of the humidifier inlet water mass flow rate on the system productivity. It shows that the productivity of the system increases with increasing value of inlet water mass flow rate of HDH unit. As shown in Fig. 10. the productivity of the SSF unit has a small increasing by increase the value of feed water mass flow rate of HDH unit. All of these findings may be explained as follows; the temperature of the water entering the humidifier is higher than the wet-bulb temperature of the air at the inlet of the humidifier. Hence, as the air is brought into contact with the water in the humidifier, the water temperature drops and wet-bulb temperature of the air leaving the humidifier at saturation state increases. So, at a constant air mass flow rate, when the water mass flow rate is increased, the dry-bulb temperature of the air leaving the humidifier increases and approaches to the temperature of the water at the inlet of the humidifier, which decreases by increasing of water mass flow rate, (i.e. the slope of the process line of the air in the humidifier increases). This means that, the moisture content of the air leaving the humidifier increases.

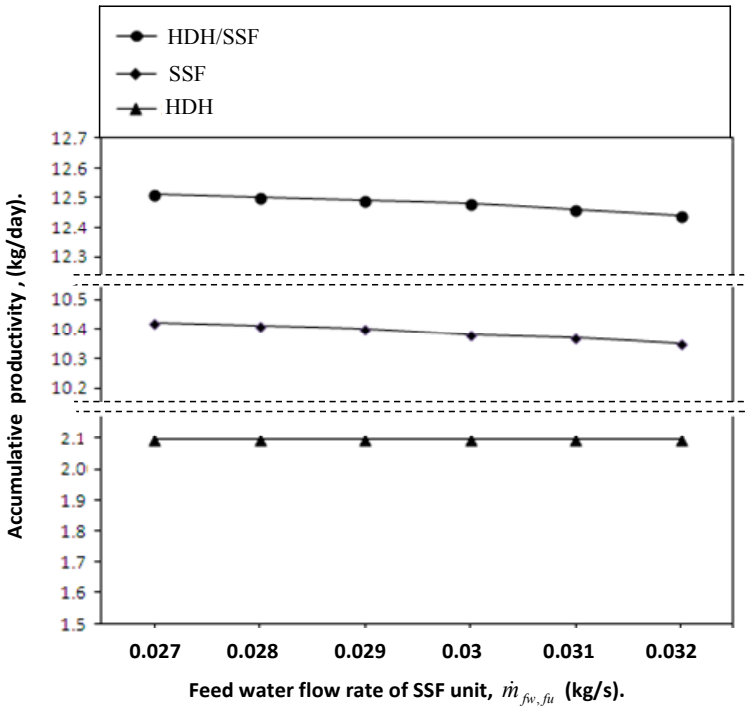

Fig. 10 Feed water mass flow rate of SSF unit with accumulative productivity.

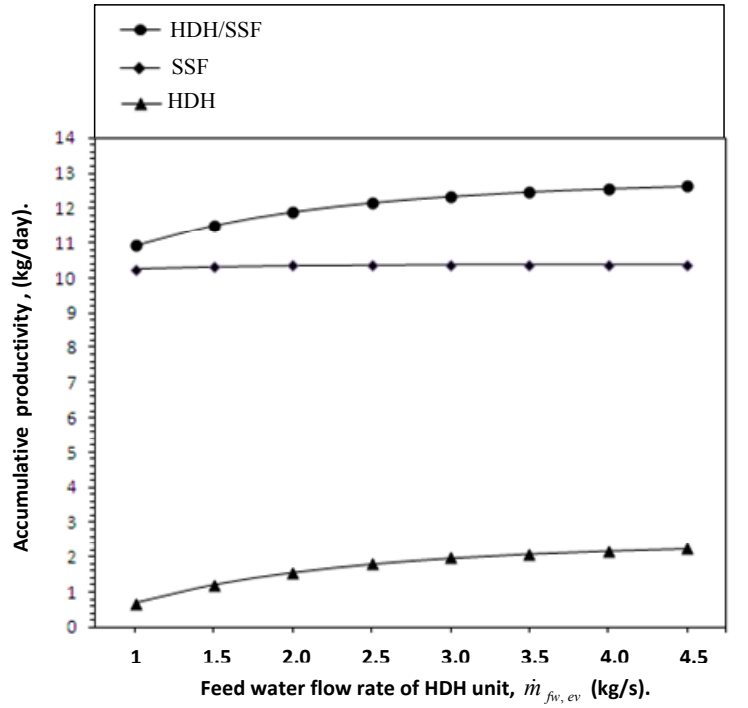

Fig. 11 Feed water mass flow rate of HDH unit with accumulative productivity.

6.5. Cooling water mass flow rate of SSF unit effect

The effect of the cooling water mass flow rate of SSF unit on the system productivity is shown in Fig. 12. It is shown that the productivity of the HDH unit is not affected by change the value of cooling water mass flow rate of SSF unit condenser, which means that increasing of hybrid system productivity is dependent only on the variation on productivity of SSF unit. By increasing the cooling water mass flow rate, significant drop in the surface temperature of the condenser tubes can be achieved which results in an increase of the rate of the condensation of the water vapor on the condenser tubes surface then, the system gives higher productivity.

6.6. Cooling water mass flow rate of HDH unit effect

The effect of the cooling water mass flow rate of HDH unit on the system productivity is shown in Fig. 13. By increasing the cooling water mass flow rate of HDH, significant drop in the surface temperature of the condenser coils can be achieved which results in an increase of the rate of the condensation of the water vapor on the condenser coils surface then, the system gives higher productivity.

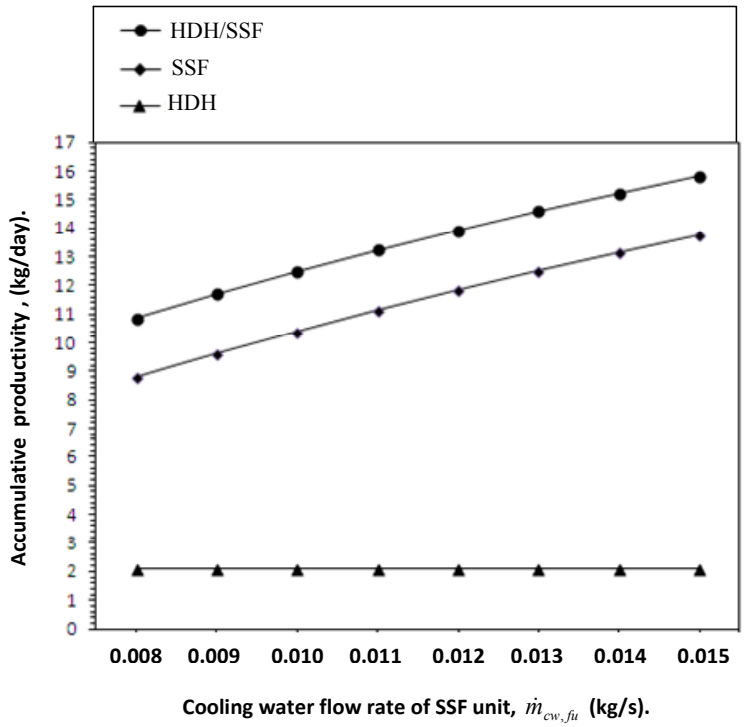

Fig. 12 Cooling water flow rate of SSF unit with accumulative productivity.

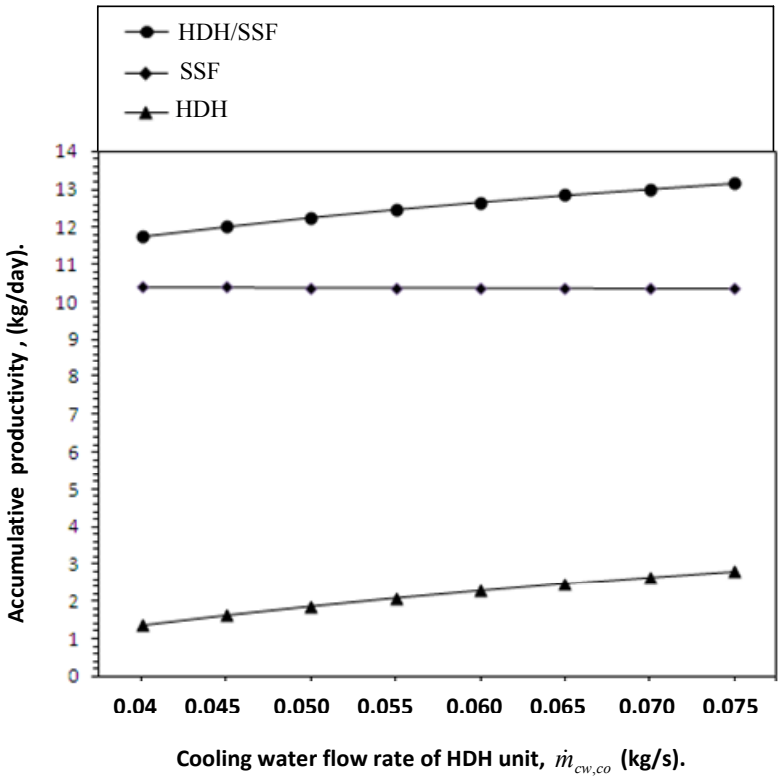

Fig. 13 Cooling water flow rate of HDH unit with accumulative productivity.

6.7. Air flow rate effect

The effect of the inlet air mass flow rate on the system productivity is given in Fig. 7. It can be observed in this figure that the productivity of the system increases by increasing the air mass flow rate to a certain value and decreases after that value. The reasons behind this behavior can be explained as follows; for the HDH unit, the wet-bulb temperature of the air at the outlet of the solar air heater decreases when the air mass flow rate is increased. In addition, at a constant water mass flow rate, dry-bulb temperature (or absolute humidity) of the air leaving the humidifier decreases and it gets closer to the wet-bulb temperature of the air at the inlet of the humidifier . For all those reasons, the rate of vaporization in the humidifier decreases, that is, moisture content of the air leaving the humidifier is reduced. In addition, at a constant cooling water mass flow rate and temperature, increased air mass flow rate increases the absolute humidity of the air leaving the dehumidifier. Consequently, they should cause a reduction in the productivity of the system, however, on the contrary the productivity of the system increases with the increasing value of air mass flow rate up to an optimum value since the air leaving the humidifier with the low moisture content carries more water vapor to the dehumidifier. The productivity of SSF unit not influenced by variation on air mass flow rate value.

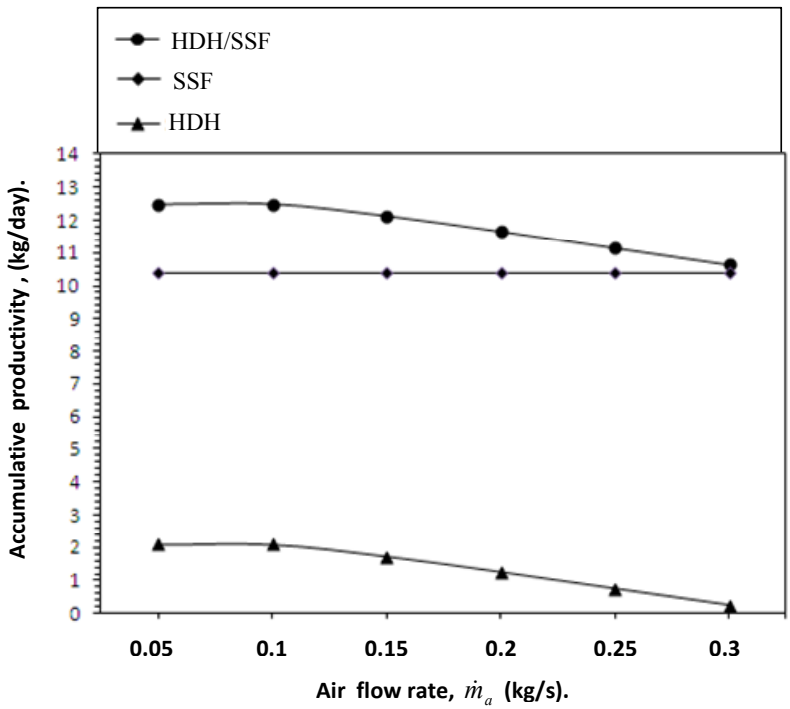

Fig. 14 Air flow rate with accumulative productivity.

6.8. Cooling water inlet temperature effect

Fig.15. shows the effect of cooling water on the fresh water production. The results showed that the mass production decreased with the increasing of the temperature cooling water. By increasing the cooling water temperature, raise in the surface temperature of the condenser tubes of both units HDH and SSF can be achieved which results in an decrease of the rate of the condensation of the water vapor on the condenser tubes surface and then lead to lower productivity of the unit.

6.9. Wind speed effect

Fig. 16. shows the effect of the wind speed on the system productivity. It can be seen from the figure that the productivity of the HDH unit is not influenced by the wind speed variations as much as the SSF unit. This result can be explained by the fact that the heat losses from the upper glass cover of collector to the ambient by convection increases with the increasing value of the wind speed. It is seen from the figure that the apparent effect of increasing the wind speed increase the productivity of the HDH unit unlike the foregoing, the reason for this may be explained as follows; the drop in productivity of SSF unit proved the mixing tank with high quantity of rejected bribe at high temperature that increase the temperature of feed water for the HDH unit, which increase its productivity.

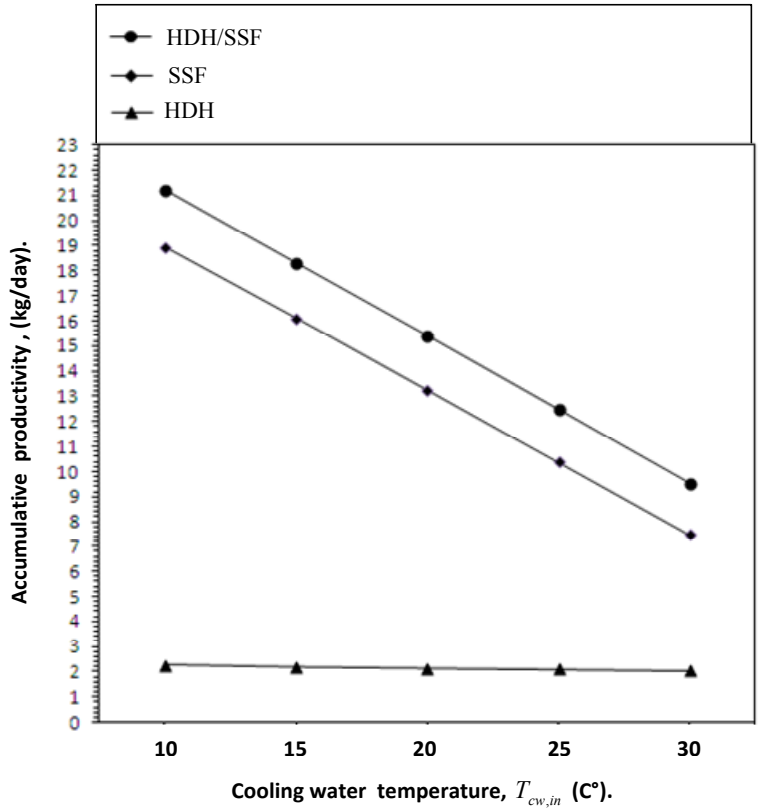

Fig. 15. Cooling water inlet temperature with accumulative productivity.

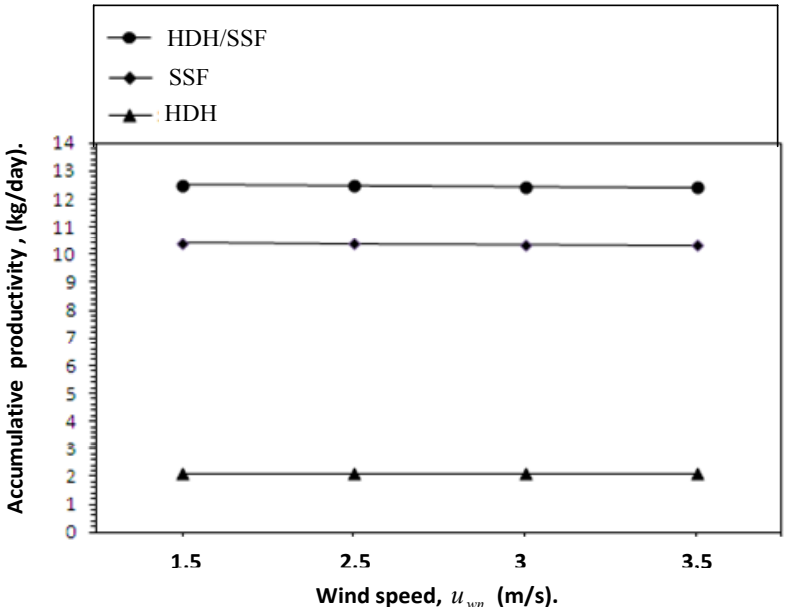

Fig. 16 Wind speed with accumulative productivity.

Ambient temperature effect

The effect of the wind speed on the system productivity present as shown in Fig. 17. The results illustrate that the system productivity increases with increasing the ambient temperature. This could be reasoned by recalling the thermal efficiency of water and air solar heaters increases with increasing the ambient.

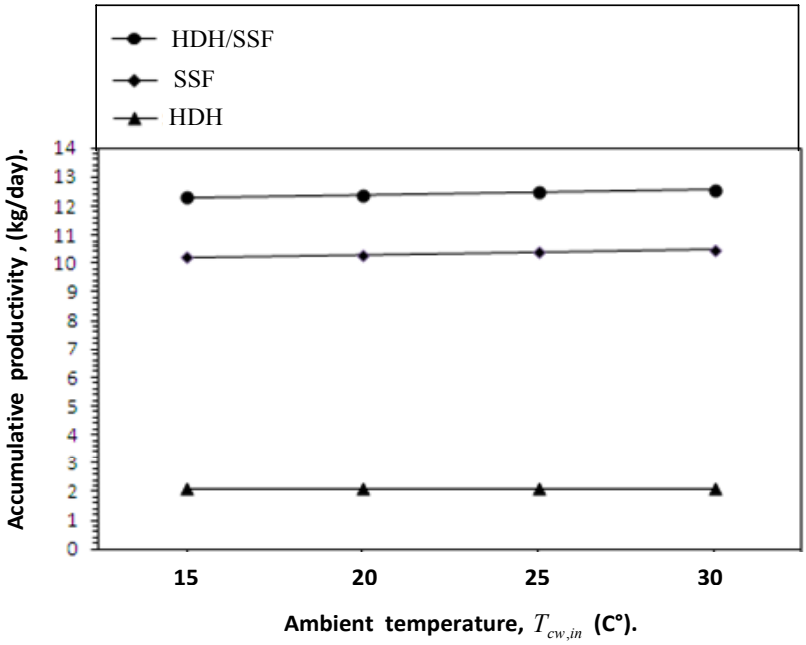

Fig. 17 Ambient temperature with accumulative productivity.

8. Conclusion

A numerical investigation was carried out with the objective of studying a hybrid desalination system consists of HDH unit and single stage flashing evaporation unit. Nine main parameters that have influence on the system productivity are the feed water salinity, feed water flow rate of SSF unit, feed water flow rate of HDH unit, cooling water flow rate of SSF unit, cooling water flow rate of HDH unit, air flow rate, cooling water temperature, wind speed and ambient temperature. The main conclusions are summarized:

1. A significant improvement on the HDH unit and SSF unit productivity can be achieved by hybridization.
2. The HDH unit and SSF unit productivity influenced by heat recovery when using mixing tank.
3. The feed water salinity, wind speed and ambient temperature have a small impact on fresh water production.
4. The system production can be increased as follow:
   - Increase cooling water flow rate and decrease its temperature.
   - Increase feed water mass flow rate of HDH unit.

9. References

[1] J.A. Dean, 2001, "Lange's Handbook of Chemistry", 15th ed., McGraw Hill, New York.

[2] Shaobo Hou, Hefei Zhang, 2008, " A hybrid solar desalination process of the multi-effect humidification dehumidification and basin-type unit", *Desalination*, Vol. 220, pp. 552–557.

[3] Garg HP, Adhikari RS, Kumar Rakesh, 2002, "Experimental design and computer simulation of multi-effect humidification-dehumidification solar distillation", *Desalination*, Vol. 153, pp. 81-86.

[4] G. Prakash Narayan, Mostafa H. Sharqawy, John H. Lienhard V, Syed M. Zubair, 2010," Thermodynamic analysis of humidification dehumidification desalination cycles", *Desalination and Water Treatment*, Vol. 16, pp. 339–353.

[5] A. Safwat Nafey, M.A. Mohamad, S.O. El-Helaby, M.A. Sharaf, 2007," Theoretical and experimental study of a small unit for solar desalination using flashing process", *Energy Conversion and Management*, Vol. 48, pp. 528–538.

[6] Hasan Baig, Mohamed A. Antar, Syed M. Zubair, 2010," Performance characteristics of a once-through multi-stage flash distillation process", *Desalination and Water Treatment*, Vol. 13, pp. 174–185.

[7] Yan Junjie, Zhang Dan, Chong Daotong, Wang Guifang, Li Luning, 2010, " Experimental study on static/circulatory flash evaporation", *International Journal of Heat and Mass Transfer* , Vol. 53, pp. 5528–5535.

[8] Mohammad Abutayeh and D. Yogi Goswami, 2009, "Solar Flash Desalination Under Hydrostatically Sustained Vacuum", *Journal of Solar Energy Engineering*, Vol. 131 / 031016, pp. 1-7.

[9] K. Onda, H. Takechi, and Y. Okumoto, 1968, " Mass transfer coefficients between gas and liquid phases in packed columns ", *Journal of Chemical Engineering of Japan*, Vol. 1, pp. 56-62.

[10] H.T. El-Dessouky, H. M. Ettouney, 2002, *"Fundamentals of Salt water Desalination*", 1st Edition, ELSEVIER.

[11] Duffie, J.A. and Beckman, W.A., 2006, *" Solar Engineering of Thermal Processes* ", 3rd Edition, Toronto, John Wiley.

[12] H. Kazeminejad, 2002," Numerical analysis of two dimensional parallel flow flat-plate solar collector", *Renewable Energy*, Vol. 26, pp. 309–323.

[13] Strigle, R. F., 1994, "Packed Tower Design and Applications, Random and Structured Packings", 2nd ed., Gulf Publishing Company.

[14] James F. Klausner, Mohamed Y. Darwish and Renwei Mei, 2003, "Computational Method and Design of A Packed Bed Diffusion Tower for the Desalination of Seawater", Proceedings of 2003 ASME Summer Heat Transfer Conference July 21-23, , Las Vegas, Nevada, USA.

[15] Warren J. Lyman, William F. Reehl and David H. Rosenblatt, 1990. "Handbook

of Chemical Property Estimation Methods", 1st edition, American Chemical Society.

[16] W.A. Khan, J.R. Culham, M.M. Yovanovich, 2006, " Convection heat transfer from tube banks in crossflow: Analytical approach ", *International Journal of Heat and Mass Transfer,* Vol. 49, pp. 4831–4838.

[17] Faye C. McQuiston, Jerald D. Parker, and JeffreySpitler, 2005, ″ Heating Ventilating and Air Conditioning Analysis and Design″, 6th Edition, John Wiley& Sons, Inc.

[18] ASHRAE, 2009, *″ Fundamental Handbook″*.

[19] Yunus A. Çengel, 2007, " Heat and Mass Transfer: A Practical Approach ", 3rd Edition, McGraw Hil.

[20] W.H. McAdams,1954, "Heat Transmission", 3rd Edition, McGraw-Hill, New York.

[21] Bashria A, A. Yousef and Adam N. M, K Sopian, A. Zaharim and M. Alghoul, 2007, "Analysis of Single and Double Passes V-Grooves Solar Collector With and Without Porous Media", *International Journal of Energy and Environment*, Issue 2, Vol. 1, pp. 109 – 114.

Nomenclatures

Latin Symbols

A	area, m^2
q	energy gain, W/m^2
C_p	specific heat, J/kgK
x	water salinity, *ppm*
g	gravitational constant, m^2/s
e	absorber plate to cover spacing and absorber plate to back plate spacing , m
D	Diffusivity coefficient, m^2/s
h	heat transfer coefficient, W/m^2K
R	universal gas constant = 8.3145 $J/mol.K$
Re	Reynolds number $\equiv \frac{\rho u d}{\mu}$, *dimensionless*
I	solar radiation rate, W/m^2
d	diameter, m
H	height, m
L	length, m
W	width, m
K	thermal conductivity, W/mK
F_R	collector heat removal factor, *dimensionless*
P	total system pressure, N/m^2
S	actual absorbing radiation solar energy, W/m^2
Pr	Prandtl number $\equiv \frac{C_p \mu}{K}$, *dimensionless*

U heat loss coefficient, W/m^2K
$\dot{m}$ Mass flow rate, kg/s
j Number of intervals or elements
s salt concentration, kg_{salt}/kg_{water}
Ra Rayleigh number $\equiv \frac{C_p \mu}{K}$, *dimensionless*
u velocity, m/s
p pressure, N/m^2
M mass flow rate per unit area, $kg/s\ m^2$
a area of heat transfer or mass transfer surface per unit of packing volume, $m^2/\ m^3$
a_{ss} Specific Surface area of the packing, $m^2/\ m^3$
k mass transfer coefficient, $kg\ m^2/s$
T Temperature, K or ◦C
$\overline{T}$ Average temperature, ◦C
F_a arrangement factor
S_D diagonal pitch, m
S_L longitudinal distance between two consecutive tubes, m
S_T transverse distance between two consecutive tubes, m
A_o minimum free-flow (or open) area on one fluid side of an exchanger, m^2
A_f fin or extended surface area on one side of the exchanger, m^2
A_p primary surface area on one side of an exchanger, m^2
N_{fin} number of fins per unit length in the fin pitch direction, $1/m$
S_F Spacing between fin plates, m
l_L dimensionless longitudinal pitch $\equiv S_L/d_o$
L_T dimensionless transverse pitch $\equiv S_T/d_o$
d_e Equivalent diameter, m
M_V Water vapor molecular weight = 18.02 *gm/mole.*
H' Henry's law constant, $Pa.m^3/mol$

Greek Symbols

α solar absorptance of collector plate , *dimensionless*
α' thermal diffusivity
β collector tilt angle, *degree*
β' volumetric coefficient of expansion, K^{-1}
υ kinetic viscosity, m^2/s
ε' Emittance factor
ω humidity ratio, $kg_{water\ vapor}/kg_{dry\ air}$

ζ	Packing void fraction, m^3/m^3
μ	dynamic viscosity, *kg/m.s*
ρ	density, kg/m^3
σ	Stefan–Boltzmann constant $= 5.67\times10^{-8}$ W/m^2K^4.
σ'	Surface tension, *N/m*
τ	solar transmittance of glazing
δ	thickness, *m*
θ	V-groove angle, *degree*

Subscripts

1	object 1
2	object 2
a	air
w	fresh water
h	hydraulic
f	Fluid or flow
ac	air solar collector
wc	water solar collector
c	convection
t	top
am	ambient
o	out
r	radiation
in	in
p	heat-absorbing plate
lb	local base
b	bottom
bi	back insulation
e	edge
g1	First (top) layer of the glass cover
g2	Second (lower) layer of the glass cover
u	useful
row	row
m	mean
L	overall
s	saturation
H	heat transfer
M	mass transfer
v	vapor
V	V-groove
fg	difference between the saturated vapor and saturated liquid values of the same
i	interface
cf	Condensate film
gc	glass cover
j	Node index

bo bond
hot Hot
cold Cold
loss loss
sw sea water
bf base fluid
np nano particle
iw inside wall
cf condensate film
cs cross sectional
cw Cooling water
ha humid air
P packing
0 property evaluated at 0 °C
cr critical
sr surface
wn wind
T total
pc pipe cell
d dry

evap evaporation
w-a from water to air
dis distillate
fin fin
an annulus
coil coil
sh shell

ev humidifier
co dehumidifier
calcu calculated
guess guessed
sc swirl chamber
or orifice
noz nozzle
as Air channel
ap Aperture
fu Flashing unit
bp Brine pool
conv Conventional
lm Log mean
ss Specific Surface
wet Wet

OG Overall gas-phase transfer units
wf Water film
eq equilibrium
su Superheat
rv removal

Superscripts

e estimated
g guessed

Acronyms and abbreviations

HDH Humidification–Dehumidification
GOR Gained Output Ratio
CFD Computational Fluid Mechanics
MENA Middle East and North Africa
MEDA Mediterranean & Middle East countries
EU European Union
NEF Non-Equilibrium Fraction
MSF Multi-Stage Flash
SSF Single-Stage Flash
BPE Boiling Point Elevation
FPSC Flat plate Solar Collector

Appendix

- Onda's correlation under-predicted the wetted specific area of the packing material.

$$a_{wet} = a_{ss,P}\left\{1-\exp\left[-1.45\left(\frac{\sigma'_{c,P}}{\sigma'_w}\right)^{0.75}\left(\frac{M_w}{a_{ss,P}\mu_w}\right)^{0.1}\left(\frac{M_w^2\, a_{ss,P}}{g\,\rho_w^2}\right)^{-0.05}\left(\frac{M_w^2}{\rho_w\sigma'_w\, a_{ss,P}}\right)^{0.2}\right]\right\}$$

The above correlation applies under the following conditions:

$$0.04 < \frac{M_w}{a_{ss,P}\mu_w} < 500\,,\ 2.5\times10^{-9} < \frac{M_w^2\, a_{ss,P}}{g\,\rho_w^2} < 1.8\times10^{-2}$$

$$1.2\times10^{-8} < \frac{M_w^2}{\rho_w\sigma'_w\, a_{ss,P}} < 0.27\,,\ 0.3 < \frac{\sigma'_{c,P}}{\sigma'_w} < 2$$

- **Water-side mass transfer coefficient (from water to interface): k_w**

$$k_w = 0.0051\left(\frac{g\,\mu_w}{\rho_w}\right)^{1/3}\left(\frac{M_w}{a_{wet}\mu_w}\right)^{2/3}\left(\frac{\rho_w D_w}{\mu_w}\right)^{1/2}\left(a_{ss,P}\,d_p\right)^{0.4}$$

- **Air-side mass transfer coefficient (from interface to air):** k_a

$$k_a = C\left(\frac{a_{T,P}D_a}{RT_a}\right)\left(\frac{M_a^2}{a_{T,P}\mu_a}\right)^{0.7}\left(\frac{\mu_a}{\rho_a D_a}\right)^{1/3}\left(a_{ss,P}\,d_p\right)^{-2}\begin{cases}C=5.23 & for \quad d_p > 0.015\\ C=2.00 & for \quad d_p \le 0.015\end{cases}$$

Where $a_{ss,P}$ represents the Specific Surface area of the packing material. And (d_P) represents the particle diameter of packing material and is the diameter of a spherical packing with the same value of bed porosity ζ and $a_{ss,P}$ as the real packing in the humidifier. It is calculated by the equation:

$$d_p = \frac{6\left(1-\zeta\right)}{a_{ss,P}}$$

- **Overall mass transfer coefficient:** k_L

Overall mass transfer coefficient k_L can be found using following equation Strigle, R. F. [1994].

$$\frac{1}{a_{T,P}k_L} = \frac{RT_i}{H' a_{wet}\, k_a} + \frac{1}{a_{wet}\, k_w}$$

Where, H' is the Henry's law constant (282.37 Pa.m^3/mol), R is the universal gas constant, T_i is the temperature (K) at the air–water interface.

- **Heat transfer coefficient on air side,** h_a **(from interface to air):**

The heat transfer coefficients are computed as follows, James F. Klausner, et al [2003].

$$\frac{Nu_a}{\mathrm{Pr}_a^{1/3}} = \frac{Sh_a}{Sc_a^{1/3}},\ h_a = k_a\left(C_{p,a}\rho_a\right)^{1/3}\left(\frac{K_a}{D_a}\right)^{2/3}$$

- **Heat transfer coefficient on water side,** h_w **(from water to interface):**

As mentioned previously, James F. Klausner, et al [2003]

$$\frac{Nu_w}{\mathrm{Pr}_w^{1/2}} = \frac{Sh_w}{Sc_w^{1/2}},\ h_w = k_w\left(\rho_w C_{p,w}\frac{K_w}{D_w}\right)^{1/2}$$

- **The coefficient of diffusivity (**D_g**) in air**

The following is an empirical equation for mass diffusivity of water vapor in air, Warren J. Lyman, et al. [1990]:

$$D_g = \frac{2.26}{P}\left(\frac{T_a + 273.15}{273.15}\right)^{1.81}$$

- **Convective heat transfer coefficient in an air flow around a tubes.**

For a Reynolds number from 2,000 to 32,000, Khan et al. [2006]:

$$h_{a,co} = \frac{0.34K_{a,co}}{d_{tube,o}}F_a\,\mathrm{Pr}^{0.31}\,\mathrm{Re}_{d_o}^{0.61}$$

Where the arrangement factor (F_a)

$$F_a = 1 + \left(l_L + \frac{7.17}{l_L} - 6.52 \right) \left[\frac{0.266}{\left(l_T - 0.8 \right)^2} - 0.12 \right] \left(100 \, \mathrm{Re}_d^{-1} \right)^{0.5}$$

$$\mathrm{Re}_d = \frac{\rho_a u_{a,\max} d_{tube,o,co}}{\mu_{a,co}}$$

$$u_{a,\max} = \frac{\dot{m}_{a,co}}{\rho_{a,co} A_{o,co}}$$

$$A_{o,co} = \left(S_{T,co} - d_{tube,o,co} \right) N_{tube,row,co} L_{tube,Ps,co}$$

- **Convective heat transfer coefficient through a water flowing inside the tubes.**

In the laminar regime, the recommended correlation for predicating the average film coefficient is, McQuiston et al. [2005]:

$$h_{cw,iw,co} = 1.86 \left(\frac{K_{w,co}}{d_{tube,in,co}} \right) \left(\mathrm{Re}_{d_i} \, \mathrm{Pr} \frac{d_{tube,in,co}}{L_{tube,co}} \right)^{\frac{1}{3}} \left(\frac{\mu_{w,co}}{\mu_{w,tube,in,co}} \right)^{0.14} \quad \text{for } \mathrm{Re}_{d_i} < 2300 .$$

$$h_{cw,iw,co} = 0.116 \left(\frac{K_{w,co}}{d_{tube,in,co}} \right) \left(\mathrm{Re}_{d_i}^{2/3} - 125 \right) \mathrm{Pr}^{1/3} \left[1 + \left(\frac{d_{tube,in,co}}{L_{tube,co}} \right)^{2/3} \right] \left(\frac{\mu_{w,co}}{\mu_{w,tube,in,co}} \right)^{0.14}$$

for $2300 \le \mathrm{Re}_{d_i} \le 10^4$

$$h_{cw,iw,co} = \frac{0.023 K_{w,co} \, \mathrm{Pr}^n \, \mathrm{Re}_{d_i}^{0.8}}{d_{tube,in,co}} \quad \text{for } \mathrm{Re}_{d_i} > 10^4 , \; 0.7 < \mathrm{Pr} < 100, \text{ and } L_{tube}/d_i > 60.$$

Where

$$n = \begin{cases} 0.4, & T_{tube,in} > T_{bulk} \quad (cooling) \\ 0.3, & T_{tube,in} < T_{bulk} \quad (heating) \end{cases}$$

- **Liquid condensed film heat transfer coefficient.**

This coefficient is given by the Nusselt correlation, ASHRAE [2009]:

$$h_{cf,co} = 0.729 \left[\frac{K_{w,co}^3 \rho_{w,co} \left(\rho_{w,co} - \rho_{v,co} \right) g \, \lambda_{fg,co}^*}{\mu_{w,co} \, d_{tube,o,co} \left(T_{s,co} - T_{tube,o,co} \right)} \right]^{0.25}$$

For ($N_{Ps,tube,co}$), vertically aligned: $h_{cf,co}\big|_{N_{Ps,tube,co}} = h_{cf,co} N_{Ps,tube,co}^{-0.25}$

Coefficient of diffusivity (k_{co}), of vapor in the air.

Using the definition of heat and mass Stanton numbers, the analogy between heat and mass transfer can be expressed more conveniently as, Yunus A. Çengel [2007]:

$$h_{a,co} \cong k_{co} \, C_{p,a,co}$$

- **Heat transfer coefficients of solar air heater and water heater.**

The convection heat transfer coefficient due to wind is recommended by McAdams [1954]

$$h_{wn} = 5.7 + 3.8 u_{wn} \qquad \text{for } 0 \le u_{wn} \le 7 \quad m/s .$$

- **The radiation heat transfer coefficient**

$$h_{r,1-2}=\frac{\sigma\left(T_1+T_2\right)\left(T_1^2+T_2^2\right)}{\frac{1}{\varepsilon_1}+\frac{A_1}{A_2}\left(\frac{1}{\varepsilon_2}-1\right)}$$ Where (T_1, T_2, ε_1, ε_2, A_1, A_2) are the temperatures, emissivities and areas of the object (1) and (2) respectively.

In the V-groove, Bashria et al.[2007].

$$\varepsilon_p=\frac{2\varepsilon_{p'}}{1+\varepsilon_{p'}}$$

- The convection heat transfer coefficients for the fluid moving on the absorbing plate and on the bottom plate are recommended by Kays and Crawford [1980] as:

$h_{c,p-f}=h_{c,b-f}=\left(\frac{K_a}{d_h}\right)\times 0.0158\,\mathrm{Re}_{d_h}^{0.8}$ where (Re_{d_h})is defined as follows, $\mathrm{Re}_{d_h}=\frac{\rho_a\,\overline{u}_f d_h}{\mu_a}$

in which $\overline{u}_f$ (m/s) is the mean velocity of fluid in the channel.

The hydraulic diameter (d_h) is defined as follows:

$$d_h=\frac{4\times \textit{flow cross sectional area}}{\textit{watted perimeter}}=\frac{4W_p e}{2W_p}=2e$$

For the V-groove $d_h=\frac{2H_V\sin(\theta/2)}{1+\sin(\theta/2)}$

B.3.4. The convection heat transfer coefficient between the glass cover and the absorbing plate is calculated by, Duffie and Beckman [2006]:

$$h_{c,p-g2}=\frac{K_a\,Nu_a}{e}$$

Where

$$Nu_a=1+1.446\left[1-\frac{1708}{Ra_a\times\cos(\beta)}\right]^{+}\left\{1-\frac{1708[\sin(1.8\beta)]^{1.6}}{Ra_a\times\cos(\beta)}\right\}+\left\{\left[\frac{Ra_a\times\cos(\beta)}{5830}\right]^{0.333}-1\right\}^{+}$$

Where the plus sign in the superscript means that only positive values of the terms in the square brackets are to be used (i.e., use zero if the term is negative). This correlation is valid for tilt collector angle $0\le\beta\le 75$.

$$Ra_a=\frac{g\beta'\,\mathrm{Pr}_a}{\upsilon^2}\left(T_p-T_{g2}\right)E_{p,as}^3$$

$$\mathrm{Pr}_a=\frac{\upsilon_a}{\alpha'_a}$$

$$\alpha'_a=\frac{K_a}{\rho_a\,C_{p,a}}$$

For ideal gas, $\beta'=1/T$ (K^{-1})

The convective heat transfer coefficient in the cavity to the cover is adjusted by the ratio

of the heat transfer area to the collector aperture area, Bashria et al.[2007]:

$$h = \frac{h}{\sin(\theta/2)}$$

- **The top loss coefficient** from the collector absorber plate to the ambient is given by the following empirical equation, Duffie and Beckman [2006]:

$$U_t = \left\{ \frac{N_{gc}}{\frac{C}{T_p}\left[\frac{T_{p,m} - T_{am}}{N_{gc} + f}\right]^e} + \frac{1}{h_{wn}} \right\}^{-1} + \frac{\sigma\left(T_{p,m} + T_{am}\right)\left(T_{p,m}^2 + T_{am}^2\right)}{\left(\varepsilon'_p + 0.0059 N_{gc} h_{wn}\right)^{-1} + \frac{2N_{gc} + f - 1 + 0.13\varepsilon'_p}{\varepsilon'_{gc}} - N_{gc}}$$

Where

$C = 520\left(1 - 0.000051\ \beta^2\right)$ *for 0°<β< 70°; for 70°<β<90°, use β =70°*

$f = \left(1 + 0.089 h_{wn} - 0.1166 h_{wn}\varepsilon'_p\right)\left(1 + 0.07866\, N_{gc}\right)$

$e = 0.43\left(1 - \frac{100}{T_{p,m}}\right),\ T_{p,m}\,(K)$

The range of conditions over which Eq. (30) has been develop, is follows, H. Kazeminejad [2002]:

$320 \le T_{p,m} \le 420\ K$

$260 \le T_{am} \le 310\ K$

$0.1 \le \varepsilon'_p \le 0.95$

$0 \le u_{wn} \le 10\ m/s$

$0 \le \beta \le 90\ K$

$1 \le N_{gc} \le 3$

- **The bottom energy loss coefficient** (U_b) is given by:

$$U_b = \frac{K_{bi}}{\delta_{bi}}$$

- **The edge loss coefficient**-area product is $(UA)_e$ then the edge loss coefficient, based on the collector area ($A_{collector}$), Duffie and Beckman [2006] is:

$$U_e = \frac{(UA)_e}{A_{eff}} = \frac{K_e A_e}{\delta_e A_{eff}}$$

- **The overall heat loss coefficient** is a complicated function of the collector construction and its operating conditions, given by the following expression:

$U_{L,wc} = U_t + U_b + U_e$.

- **Boiling Point Elevation**

The correlation for the boiling point elevation of seawater is , El-Dessouky et al. [2002].

$$\mathrm{BPE} = (a_1 x + a_2 x + a_3 x) \times 10^{-4} \quad \text{(B.1)}$$

$$a_1 = 8.325 \times 10^{-2} + 1.883 \times 10^{-4} T_b + 4.02 \times 10^{-6} T_b^2$$

$$a_2 = -7.625 \times 10^{-4} + 9.02 \times 10^{-5} T_b - 5.2 \times 10^{-7} T_b^2$$

$$a_3 = 1.522 \times 10^{-4} - 3 \times 10^{-6} T_b - 3 \times 10^{-8} T_b^2$$

Where T_b is the brine temperature in °C and x is the salt concentration. The above equation is valid over the following ranges: $10000 \le x \le 20000$ *ppm*, $10 \le T \le 110$°C.

- **Non-Equilibrium Allowance**

The correlations for the non-equilibrium allowance (NEA) for the MSF system is developed through the following equation give value for NEA [°C] as a function of the chamber length, brine pool height, the water film velocity, and water film temperature drop, Y. Junjie et al. [2010];

$$NEA = erf\left[\left(\frac{H_{bp}}{2}\sqrt{\frac{\rho_{fw} C_{p,fw}}{a_1 \cdot L_{fu} / u_{wf}}}\right)^{a_2}\right]$$

where

$$a_1 = 5.43 \times 10^3 \cdot H_{bp}^{0.778} \cdot p_v^{0.558}$$

$$a_1 = 0.565\, \Delta T_{su}^{0.181}$$

$$u_{wf} = \frac{\dot{m}_{fw}}{\rho_{fw} w_{fu} H_{bp}}$$

Superheat (ΔT_{su}) represents the theoretically maximum temperature drop of water film in a given flash system and therefore is viewed as the driving force for flash phenomena

$$\Delta T_{su} = T_{fw} - T_{eq}$$

or

$$\Delta T_{su} = T_{wf} - T_{eq}$$

and

$$T_{eq} = T_s(p_{eq}).$$